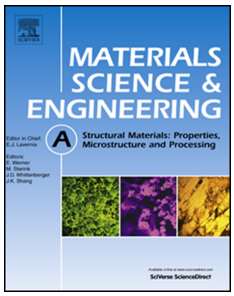

Complexity analysis of serrated flow in a bulk metallic glass under constrained and unconstrained conditions

Jamieson Brechtl, Xie Xie, Zhong Wang, Junwei Qiao, Peter K. Liaw

PII: S0921-5093(19)31371-1

DOI: https://doi.org/10.1016/j.msea.2019.138585

Reference: MSA 138585

To appear in: *Materials Science & Engineering A*

Received Date: 21 September 2019

Revised Date: 21 October 2019

Accepted Date: 22 October 2019

Please cite this article as: J. Brechtl, X. Xie, Z. Wang, J. Qiao, P.K. Liaw, Complexity analysis of serrated flow in a bulk metallic glass under constrained and unconstrained conditions, *Materials Science & Engineering A* (2019), doi: https://doi.org/10.1016/j.msea.2019.138585.

Complexity Analysis of Serrated Flow in a Bulk Metallic Glass Under Constrained and Unconstrained Conditions

Jamieson Brechtl[a], Xie Xie[b], Zhong Wang[b,c], Junwei Qiao[c], Peter K. Liaw[b,*]

[a] The Bredesen Center for Interdisciplinary Research and Graduate Education, The University of Tennessee, Knoxville TN 37996, USA

[b] Department of Materials Science and Engineering, The University of Tennessee, Knoxville, TN 37996, USA

[c] College of Materials Science and Engineering, Taiyuan University of Technology, Taiyuan 030024, China

* Corresponding author. Tel.: +1-865-974-6356

E-mail address: pliaw@utk.edu (P. K. Liaw)

Abstract

For the present work, the $Zr_{55}Cu_{30}Ni_5Al_{10}$ (atomic percent) bulk metallic glass underwent room-temperature compression experiments in both the constrained and unconstrained conditions. For the constrained condition, samples were exposed to strain rates ranging from 2×10^{-5} s^{-1} - 2×10^{-3} s^{-1}, while for the unconstrained case, the rates varied between 5×10^{-5} s^{-1} - 2×10^{-3} s^{-1}. The serrated flow was modeled and analyzed using the refined composite multiscale entropy algorithm. Findings indicate that the complexity of the serration behavior increased with respect to the strain rate for both conditions.

Keywords: modelling/simulations ; characterization ; stress/strain measurements ; amorphous materials ; plasticity

Introduction

Bulk metallic glasses (BMGs) have attracted a great deal of interest during the past several decades due to their excellent combinations of mechanical, physical, and chemical properties, such as exceptional hardness, room temperature irradiation resistance, good fatigue resistance, large elastic limits, high strength, favorable magnetic performance, wear resistance, formability, and good corrosion resistance [1-9]. Plastic strain during inhomogeneous deformation in BMGs is typically localized into a thin nanoscale region that is referred to as a shear band [10]. These types of defects are the primary force governing the mechanical behavior of this alloy system. It has been suggested that a key issue in designing ductile metallic glasses will lie in the ability to control the shear band nucleation and propagation [10, 11].

In terms of the atomic theory in BMGs, Spaepen has proposed a model where the plastic deformation results from a large amount of the stress-driven creation of free volumes by atomic jumps [12]. The local distribution of free volumes is thought to control the deformation, and the fertile sites with a higher free volume content can easily accommodate local shear strains [13]. Subsequently, Argon developed a shear-transformation theory, which hypothesized that atomic-cluster rearrangements were the basic carriers of plasticity in BMGs [14].

During compression tests, BMGs may undergo what is known as the serrated flow, which is characterized by jerky oscillations in the stress-strain graph [15]. This type of behavior is significant because it is associated with plastic instabilities that lead to considerable alterations in the microstructure [16, 17]. The serrated flow has

been observed in BMGs [18-23], as well as in numerous other structural materials, such as steels [15, 24-26], Al-Mg alloys [15, 27-33], and high entropy alloys [15, 34-39].

Complexity-based measurements, such as the multiscale entropy (MSE) algorithm, have been used to model and analyze the dynamical behavior of the serrated flow [27, 40]. As a successor to the MSE method, the refined composite multiscale entropy (RCMSE) algorithm can also model and analyze time series data [41, 42]. The RCMSE technique has two distinct advantages over its predecessor, namely that it can achieve more accurate results given the same amount of data, and it has a significantly lower chance of producing undefined entropy values [41].

The present investigation applies the RCMSE method to model and analyze the serrated flow in BMGs to achieve a link between the free-volume defects and the dynamics of the serrated flow. In doing so, it is expected that a greater understanding of the effects of strain rate and geometric constraint on the serration behavior of BMGs will be achieved. Therefore, it is anticipated that the present work will advance our fundamental understanding of the serration phenomena in BMGs.

Materials and Methods

The alloy mixture of Zr, Cu, Ni, and Al with purity higher than 99.9 weight percent (wt. %) was arc-melted in a Ti-gettered high-purity argon atmosphere to fabricate the $Zr_{55}Cu_{30}Ni_5Al_{10}$ (atomic percent, at. %) sample. Then the melted mixture was suction cast into a water-cooled copper mold to form a rectangular bar with a cross section of 3 × 3 mm. The cast rods for compression tests were prepared with a length of 6 mm (unconstrained) or 3 mm (constrained) and diameter of 3 mm. The two compression faces of each sample were then carefully polished such that they were parallel to one other.

The uniaxial compression tests were performed at room temperature using a computer-controlled MTS 810 materials testing machine at a constant strain rate. The samples compressed in the constrained condition were subjected to strain rates ranging from 2×10^{-5} s^{-1} - 2×10^{-3} s^{-1} while the specimens in the unconstrained condition underwent strain rates varying from 5×10^{-5} s^{-1} - 2×10^{-3} s^{-1}. The time, stress, and strain data were recorded, using a data-acquisition rate of 100 Hz. The data was analyzed using the RCMSE method, please see Appendix 1 for details of the algorithm.

Scanning electron microscopy (SEM) was performed to characterize the surface morphology of the fractured samples. The microscopy was achieved via a LEO Gemini 1525 field-emission scanning-electron microscope. To better understand the

effect of the sample geometry on the shear-band interactions during compression, microscopy was conducted on the samples compressed in both the constrained and unconstrained conditions.

To examine the complexity of the serrated flow, one employs the RCMSE technique. One begins this process by first eliminating the underlying strain-aging trend that occurs during plastic deformation by fitting the stress versus time data using a moving average method [24]. The trend is eliminated from the original data, and then the coarse-grained time series, $y_{k,j}^{\tau}$ [43], is constructed:

$$y_{k,j}^{\tau} = \frac{1}{\tau} \sum_{i=(j-1)\tau+k}^{j\tau+k-1} x_i \quad ; \; 1 \leq j \leq \frac{N}{\tau} \qquad 1 \leq k \leq \tau \tag{1}$$

where N is the total number of data points from the original time series, x_i is the ith point from the given stress-time series, k is an index, which denotes where to begin the algorithm in the original series, and τ is the scale factor, which ranges from 1 to 20 (τ_{max} = 20 allows for sufficient analysis of data) [44-46].

One then makes the template vectors of dimensions, m and $m + 1$:

$$\boldsymbol{y}_{\boldsymbol{k,i}}^{\boldsymbol{\tau,m}} = \left\{ y_{k,i}^{\tau} \;\; y_{k,i+1}^{\tau} \;\ldots\; y_{k,i+m-1}^{\tau} \right\} \;\; ; \;\; 1 \leq i \leq N - m \, ; \; 1 \leq k \tag{2}$$

Here m was given a value of 2 to reduce the standard error in the sample-entropy results [44]. Next, determine the number of matching template vectors [44]:

$$d_{ab}^{\tau,m} = \left\| \boldsymbol{y}_{\boldsymbol{a}}^{\boldsymbol{\tau,m}} - \boldsymbol{y}_{\boldsymbol{b}}^{\boldsymbol{\tau,m}} \right\|_{\infty} = \max\left\{ \left| y_{1,a}^{\tau} - y_{1,b}^{\tau} \right| \ldots \left| y_{i+m-1,a}^{\tau} - y_{i+m-1,b}^{\tau} \right| \right\} < r \tag{3}$$

where r is typically chosen as 0.15σ (σ is the standard deviation of the data) to ensure that the sample entropy does not depend on the variance of the original time series

[44].

The refined composite multiscale entropy values for the stress-time series are then found by [41]:

$$RCMSE(\boldsymbol{y}, \tau, m, r) = Ln\left(\frac{\sum_{k=1}^{\tau} n_{k,\tau}^{m}}{\sum_{k=1}^{\tau} n_{k,\tau}^{m+1}}\right) \quad \textbf{(4)}$$

where the variables in Eq. 4 are the same as defined for Eq. 1.

Results

Figure 1(a) presents the SEM images, which show the primary shear bands on the lateral surface after an unconstrained compression test with a strain rate of 2×10^{-4} s^{-1}. Figure 1(b) displays the amplified region, which gives a better visualization of the shear-band interactions. The same surfaces for the samples tested in the constrained condition (same strain rate) are displayed in Figs. 2(a)-(b). The specimens compressed in this condition show more shear-band intersections, as compared to the unconstrained condition.

The detrended stress vs. time data for the constrained condition with strain rates varying from 2×10^{-5} s^{-1} - 2×10^{-3} s^{-1} (room temperature) is presented in Fig. 3(a). As the strain rate increases, there is an apparent decrease in the time between successive avalanches. Furthermore, the stress fluctuations display more irregularity as the strain rate rises. For the lowest strain rate, the magnitude of the large stress-stress drops, is significantly larger, as compared to the other strain rates.

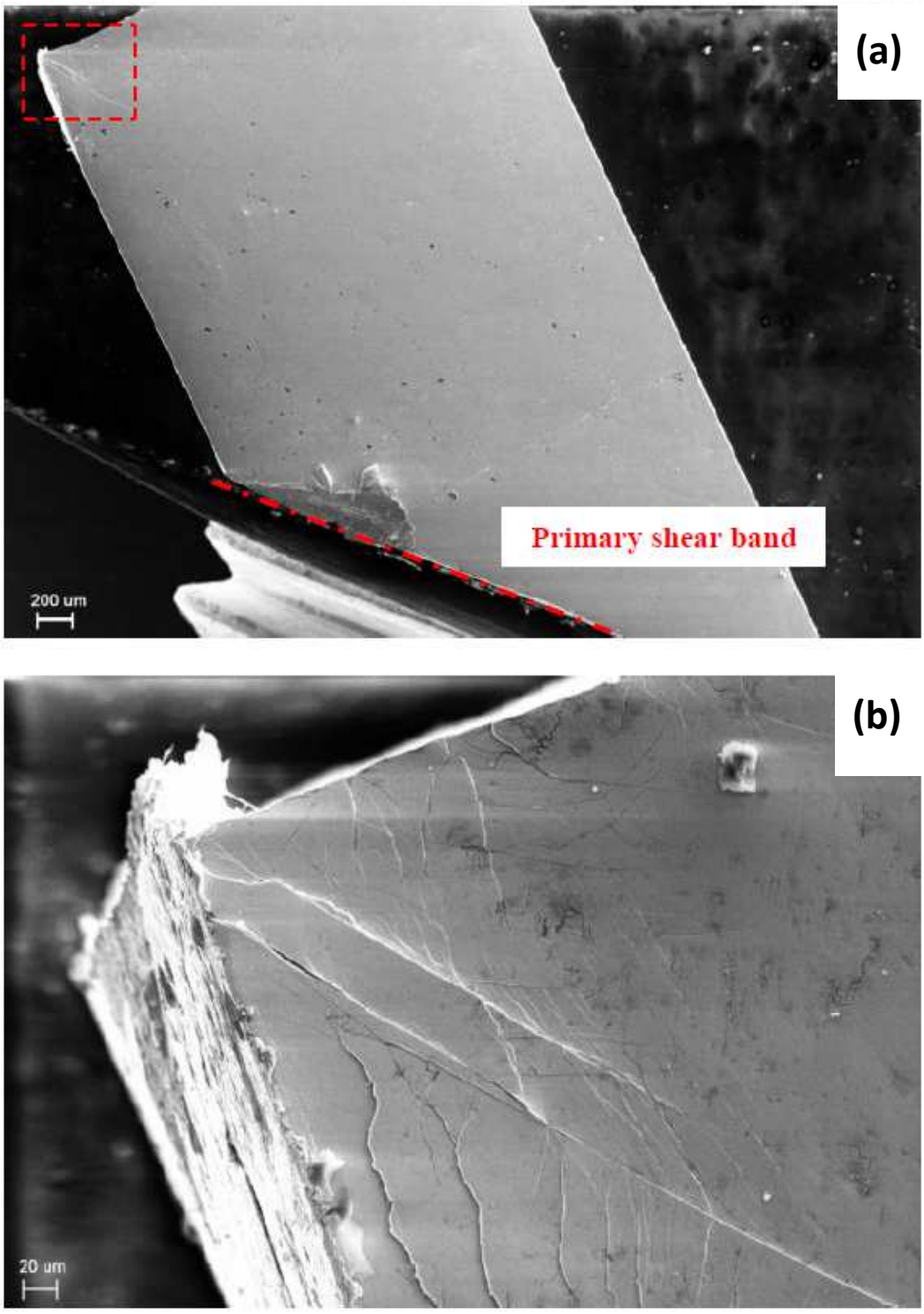

Fig. 1. (a) SEM image showing the primary shear bands (fracture plane, indicated as a red dash-dot line) on the lateral surface after the unconstrained compression at the strain rate of 2×10^{-4}/s, and (b) the amplified region showing the interaction of shear bands (From Ref. [47]).

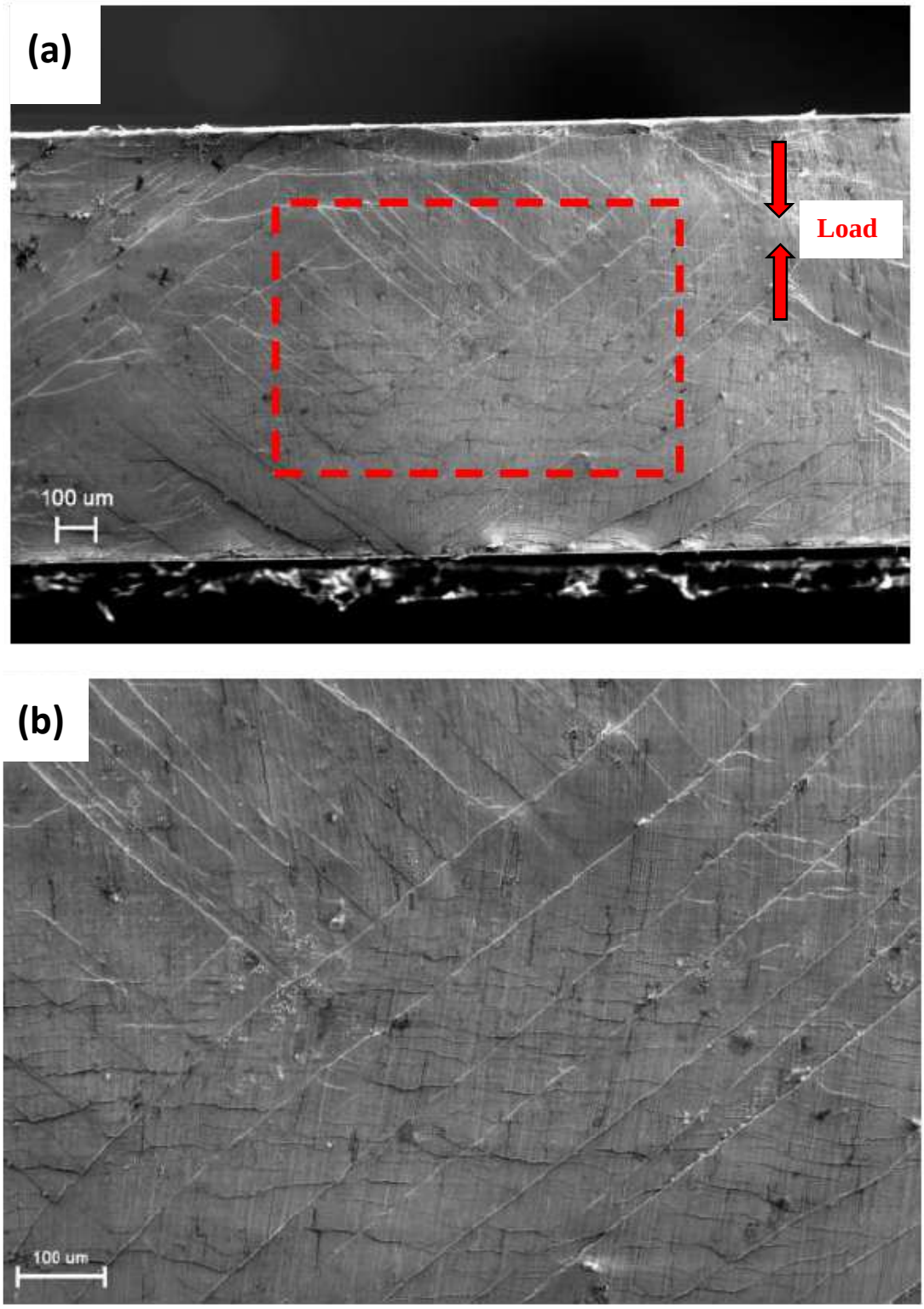

Fig. 2. (a) SEM image showing the multiple shear bands on the lateral surface after constrained compression at a strain rate of 2×10^{-4} s^{-1} and (b) the amplified region (red box) showing the interaction of shear bands (From Ref. [47]).

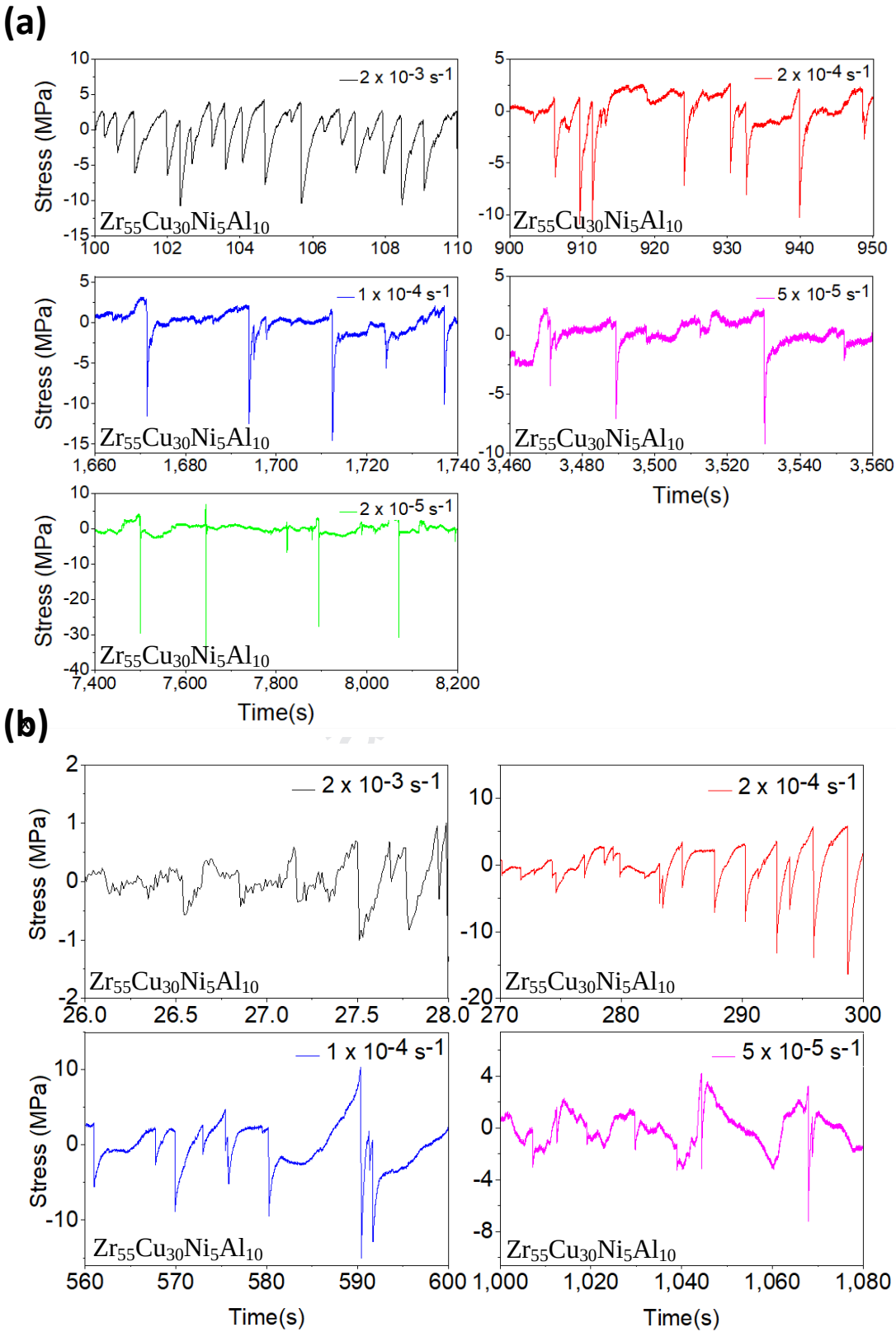

Fig. 3. The detrended stress vs. time for the Zr-based BMG compressed in the (a) constrained condition with strain rates ranging from 2×10^{-5} s^{-1} - 2×10^{-3} s^{-1} and (b) unconstrained condition with strain rates varying from 5×10^{-5} s^{-1} - 3×10^{-3} s^{-1}.

Figure 3(b) displays the fluctuations for the unconstrained condition with strain rates of 5×10^{-5} s^{-1} - 2×10^{-3} s^{-1}. The serrations appear to have a more irregular structure, relative to the constrained condition. However, like the constrained condition, the time between successive drops observes a decreasing trend.

Figure 4(a) presents the results of the sample entropy (complexity) modeling and analysis for the Zr BMG compressed in the constrained conditions. As observed, the sample-entropy curve increases with increasing strain rate. For a strain rate of 2×10^{-3} s^{-1}, the sample entropy monotonically increased with increasing the scale factor, τ. In contrast, the samples compressed at strain rates ranging from 2×10^{-5} s^{-1} - 2×10^{-4} s^{-1} initially exhibited decreasing complexity for lower τ and subsequently showed increasing complexity with increasing τ. Furthermore, the range of scale factors in which there was a minimum sample-entropy value increased with increasing the strain rate. Finally, the sample entropy for the highest strain rate was significantly larger at all scale factors, relative to the other strain-rate conditions.

The sample-entropy curves for the specimens compressed in the unconstrained condition for strain rates of 5×10^{-5} s^{-1} - 2×10^{-3} s^{-1} are displayed in Fig. 4(b). For the constrained condition, the sample-entropy curves increased with an increasing strain rate, in general. Additionally, the decreasing trend for the complexity at lower scale factors (strain rates less than 2×10^{-3} s^{-1}) is significantly more pronounced, relative to the results for the constrained sample geometry, as summarized in Fig. 4(a).

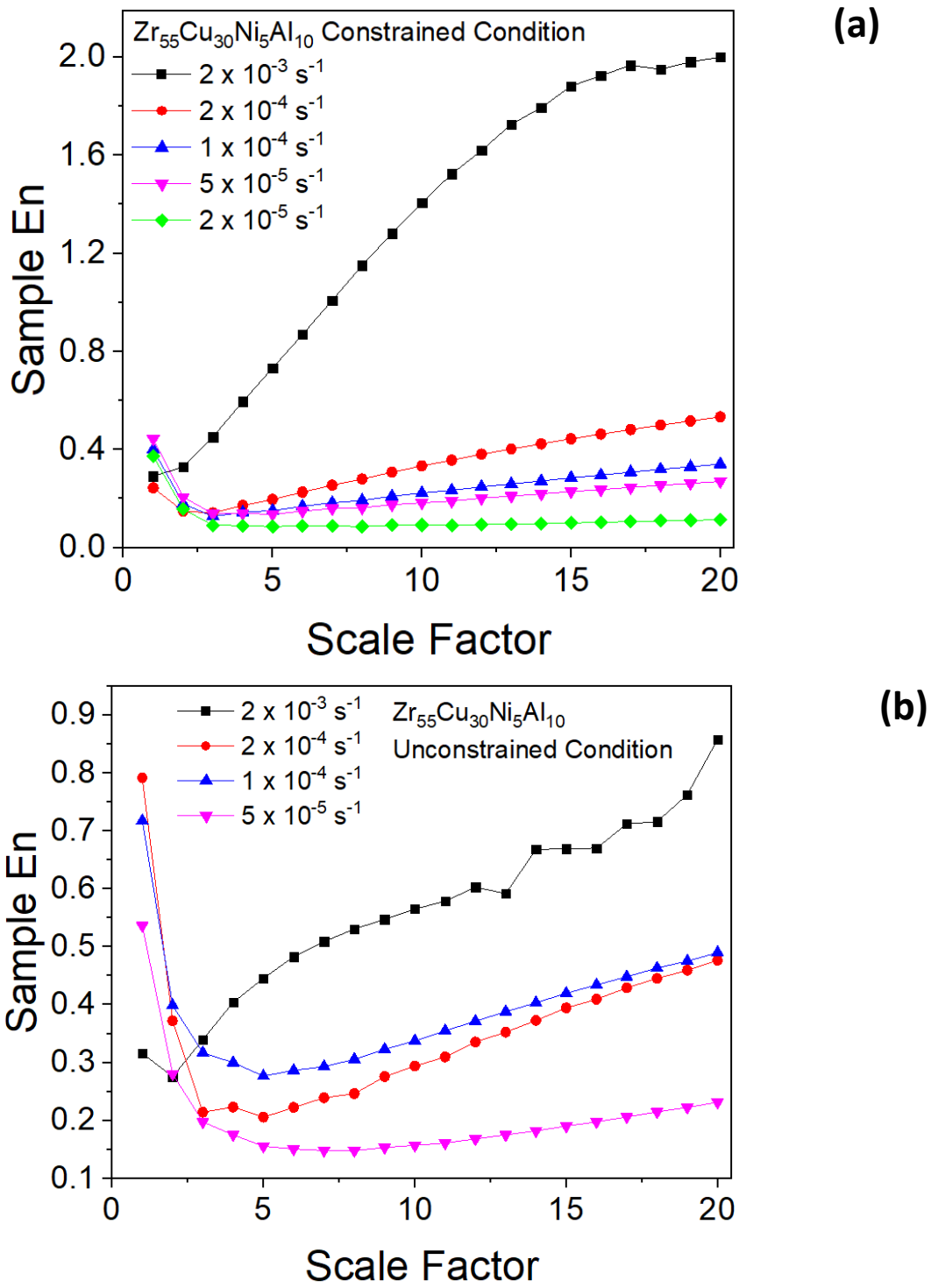

Fig. 4. Sample-entropy results for the Zr-based BMG compressed in the (a) constrained condition with strain rates ranging from 2×10^{-5} s^{-1} - 2×10^{-3} s^{-1} and (b) unconstrained condition with strain rates varying from 5×10^{-5} s^{-1} - 3×10^{-3} s^{-1}.

In Figs. 4(a)-(b), the sample-entropy curves were comparable for strain rates lower than 2×10^{-3} s^{-1}. At this strain rate, however, there was a pronounced difference between the sample-entropy curves for both conditions at $\tau = 20$. Here, the sample entropy was ~ 2.0 for the constrained condition, while it was ~ 0.85 in the unconstrained condition.

Discussion

As mentioned previously, the sample-entropy curves for the constrained condition were noticeably different, relative to the unconstrained condition [see Figs. 4(a)-(b)]. In contrast to the constrained condition, the sample entropy was greater for lower τ for the unconstrained condition for strain rates greater than 2×10^{-5} s^{-1}. The higher sample entropy at lower scale factors suggests that there is a higher degree of "meaningful structural richness" [44] in the serrated flow occurring over a shorter time period. This richness in the dynamics may correspond to stress fluctuations that are more spatially correlated.

For white noise, the sample entropy values also decreases at lower scales [46]. Since this type of noise is comprised of the highly-uncorrelated behavior, this trend suggests that in the unconstrained condition, the Zr BMG undergoes serrations that behave more randomly. Furthermore, the decreasing trend in the complexity may arise from a lower signal to noise ratio due to a reduced number of data points caused by lower fracture times for the unconstrained condition [44]. This relatively-shorter time until failure may arise from the absence of a boundary effect in

the unconstrained condition, where the successive triggering of weak spots can occur at a relatively-faster rate [47].

The rise in the sample entropy for the unconstrained condition [see Fig. 4(b)] at larger τ indicates that despite the pronounced decrease in the sample-entropy at lower values, the serrated flow still exhibits the complex behavior across multiple time-scales [44, 45]. Interestingly, the decreasing and increasing trends, as discussed above, is absent for the constrained condition, indicating that the serrated flow for this condition is more complex in nature.

As discussed in [48-50], metallic glasses are regarded as a topologically-disordered material that contains soft-zone defects. These defects are similar to liquid-like sites, which are lower in density and contain higher free volumes [51] as compared to the matrix. These lower-density regions are coupled with more condensed regions that are known as the anti-free volume, or p-type defects [51, 52]. Furthermore, during compression, the free volume content (and soft zone defects) in an amorphous alloy increases with an increase in the strain rate [53]. To compensate for an increase in the quantity of soft zones, there will also be an increase in the p-type defects in the matrix.

Importantly, an increase in the local concentration of free volumes will eventually lead to the creation of voids that can spontaneously coalesce into microcracks [54]. Thus, with an increasing deformation rate, there should be a rise in the variety of interactions between adjacent microcracks in the matrix. This increase in the variety of interactions should consequently lead to serrated flow that exhibits more complex

behavior.

Therefore, an increase in the dynamical complexity of the serration behavior with increasing the strain rate appears to be linked to an enhanced frequency of defect creation at the higher strain rate [53]. Thus, a higher strain rate will lead to a greater number of both soft-zone and jam-zone defects that can interact with propagating microcracks during the serrated flow. This enhancement in the variety of interactions is reflected by the results of the RCMSE modeling and analysis where it increases for the higher compression rates, as presented in Figs. 4(a)-(b). Therefore, as the density of defects increases in the alloy, the serrations will contain underlying dynamics that are of a more complex nature.

At a strain rate of 2×10^{-4} s^{-1}, scanning electron microscopy revealed a higher density of shear-band intersections in multiple directions for the sample compressed in the constrained condition, relative to the unconstrained condition [47]. Combining the above result with the data shown in Figs. 4(a)-(b) suggests that at the given strain rate, the increased density of shear bands in the constrained condition is associated with a higher frequency of relatively-larger stress drops. This prolonged drop in the stress may be linked to an avalanche event where a weak spot may trigger other weak spots to slip [55] for a longer period of time.

Therefore, in this context, the higher sample entropy of the serrated flow at a strain rate of 2×10^{-3} s^{-1} may correspond to weak spots that are more spatially linked, in general. In this sense, the complexity may gauge the ability of weak spots to "communicate" with one another during an avalanche. The higher sample-entropy

curve in the constrained condition at a rate of 2×10^{-3} s^{-1} suggests that the defect interactions have a greater effect on the complexity of the serrated flow at higher strain rates. Furthermore, the samples also underwent compression for a longer time before rupture [see Figs. 3(a)-(b)] in the constrained condition. The combination of generally-higher sample entropy values, increased shear-band densities (in the constrained condition), and sample lifetimes, suggests that an increase in the complexity may correspond to an increased ability of the alloy to adapt [44] to an applied load.

Furthermore, the complexity of the serrated flow was the highest in the constrained condition for a strain rate of 2×10^{-3} s^{-1}, which indicates higher spatiotemporal correlations between slipping weak spots during an avalanche. The SEM imaging revealed a higher density of shear-band interactions during the serrated flow for the sample compressed in the constrained condition. The microscopy results combined with the complexity analysis support the idea that the serration events, which correspond to defect interactions, are more spatially correlated in the constrained condition. Furthermore, the higher sample entropy at the highest strain rate indicates that defect interactions have a greater effect on the dynamical complexity.

Conclusions

For the present work, the $Zr_{55}Cu_{30}Ni_5Al_{10}$ bulk metallic glass underwent room-temperature compression tests in both constrained and unconstrained conditions at

strain rates ranging from 2×10^{-5} s^{-1} - 2×10^{-3} s^{-1}. The complexity of the serration behavior was found to increase with increasing the strain rate for both conditions. This increase in the sample entropy with increasing the strain rate is thought to be due to an increase in the number of interactions among the free volumes, anti-free volume defects, cracks, and shear bands in the alloy during plastic deformation. Furthermore, the complexity of the serrated flow was the highest in the constrained condition for a strain rate of 2×10^{-3} s^{-1}, which indicates higher spatiotemporal correlations between slipping weak spots during an avalanche. The SEM imaging revealed a higher density of shear-band interactions during the serrated flow for the sample compressed in the constrained condition. The microscopy results combined with the complexity analysis support the idea that the serration events, which correspond to defect interactions, are more spatially correlated in the constrained condition. Furthermore, the higher sample entropy at the highest strain rate indicates that defect interactions have a greater effect on the dynamical complexity.

Acknowledgements

We gratefully acknowledge the support of the US National Science Foundation (NSF) through grants DMR 1611180 and 1809640, the Department of Energy (DOE), DE-FE-00011194 with Drs. Shiflet, Farkas, Cedro, Mullen, and Reinit as contract monitors.

Author contributions

All authors contributed extensively to the work presented in this manuscript. X.X. and Z.W. prepared the samples and performed the compression testing. The analysis of the stress-time data was done by J.B. J.B., X.X., J. Q., and P.K.L. wrote the main components of the manuscript while all authors discussed the results and commented on the manuscript at all stages of preparation.

Competing financial interests

The authors declare that they have no competing financial interests.

Correspondence and requests for materials should be addressed to P. K. L. (pliaw@utk.edu)

Data Availability

The raw/processed data required to reproduce these findings cannot be shared at this time due to legal or ethical reasons.

References

[1] C.A. Schuh, T.C. Hufnagel, U. Ramamurty, Overview No.144 - Mechanical behavior of amorphous alloys, Acta Materialia 55(12) (2007) 4067-4109.

[2] M.W. Chen, Mechanical behavior of metallic glasses: Microscopic understanding of strength and ductility, Annu. Rev. Mater. Res. 38(1) (2008) 445-469.

[3] S.V. Madge, A. Caron, R. Gralla, G. Wilde, S.K. Mishra, Novel W-based metallic glass with high hardness and wear resistance, Intermetallics 47 (2014) 6-10.

[4] A.L. Greer, K.L. Rutherford, I.M. Hutchings, Wear resistance of amorphous alloys and related materials, Int. Mater. Rev. 47(2) (2002) 87-112.

[5] W.H. Peter, R.A. Buchanan, C.T. Liu, P.K. Liaw, M.L. Morrison, J. C. A. Carmichael, J.L. Wright, Localized corrosion behavior of a zirconium-based bulk metallic glass relative to its crystalline state, Intermetallics 10(11-12) (2002) 1157-1162.

[6] G.Y. Wang, P.K. Liaw, M.L. Morrison, Progress in studying the fatigue behavior of Zr-based bulk-metallic glasses and their composites, Intermetallics 17(8) (2009) 579-590.

[7] G.Y. Wang, M.D. Demetriou, J.P. Schramm, P.K. Liaw, W.L. Johnson, Compression-compression fatigue of $Pd_{43}Ni_{10}Cu_{27}P_{20}$ metallic glass foam, J. Appl. Phys. 108(2) (2010).

[8] F. Luo, F. Sun, K.S. Li, F. Gong, X. Liang, X.Y. Wu, J. Ma, Ultrasonic assisted micro-shear punching of amorphous alloy, Mater. Res. Lett. 6(10) (2018) 545-551.

[9] J. Brechtl, S. Agarwal, M.L. Crespillo, T. Yang, H. Bei, S.J. Zinkle, Evolution of the microstructural and mechanical properties of BAM-11 bulk metallic glass during ion irradiation and annealing, J. Nucl. Mater. 523 (2019) 299-309.

[10] A.L. Greer, Y.Q. Cheng, E. Maj, Shear bands in metallic glasses, Materials Science and Engineering: R: Reports 74(4) (2013) 71-132.

[11] V. Schnabel, J. Bednarcik, D. Music, T. Pazur, C. Hostert, J.M. Schneider, Temperature-induced short-range order changes in $Co_{67}B_{33}$ glassy thin films and elastic limit implications, Mater. Res. Lett. 3(2) (2015) 82-87.

[12] F. Spaepen, A microscopic mechanism for steady state inhomogeneous flow in metallic glasses, Acta Metall. Mater. 25 (1977) 407-415.

[13] K. Maeda, S. Takeuchi, Computer simulation of deformation in two‐dimensional amorphous structures, Physica status solidi (a) 49(2) (1978) 685-696.

[14] A. Argon, Plastic deformation in metallic glasses, Acta metallurgica 27(1) (1979)

47-58.

[15] Y. Zhang, J.P. Liu, S.Y. Chen, X. Xie, P.K. Liaw, K.A. Dahmen, J.W. Qiao, Y.L. Wang, Serration and noise behaviors in materials, Progress in Materials Science 90 (2017) 358-460.

[16] Y. Zhang, T.T. Zuo, Z. Tang, M.C. Gao, K.A. Dahmen, P.K. Liaw, Z.P. Lua, Microstructures and properties of high-entropy alloys, Prog. Mater. Sci. 61 (2014) 1-93.

[17] S. Niu, H. Kou, Y. Zhang, J. Wang, J. Li, The characteristics of serration in $Al_{0.5}$CoCrFeNi high entropy alloy, Materials Science and Engineering A 702 (2017) 96-103.

[18] J. Antonaglia, X. Xie, G. Schwarz, M. Wraith, J. Qiao, Y. Zhang, P.K. Liaw, J.T. Uhl, K.A. Dahmen, Tuned critical avalanche scaling in bulk metallic glasses, Sci Rep 4 (2014) 4382.

[19] J.W. Qiao, Y. Zhang, P.K. Liaw, Serrated flow kinetics in a Zr-based bulk metallic glass, Intermetallics 18 (2010) 2057-2064.

[20] W.H. Jiang, F. Jiang, F.X. Liu, H. Choo, P.K. Liaw, Temperature dependence of serrated flows in compression in a bulk-metallic glass, Applied Physics Letters 89 (2006).

[21] W.H. Jiang, G.J. Fan, F.X. Liu, G.Y. Wang, H. Choo, P.K. Liaw, Rate dependence of shear banding and serrated flows in a bulk metallic glass, J. Mater. Res. 21(9) (2006) 2164-2167.

[22] J.W. Qiao, H.L. Jia, C.P. Chuang, E.W. Huang, G.Y. Wang, P.K. Liaw, Y. Ren, Y. Zhang, Low-temperature shear banding for a Cu-based bulk-metallic glass, Scr. Mater. 63(8) (2010) 871-874.

[23] X. Xie, Y.-C. Lo, Y. Tong, J. Qiao, G. Wang, S. Ogata, H. Qi, K.A. Dahmen, Y. Gao, P.K. Liaw, Origin of serrated flow in bulk metallic glasses, J. Mech. Phys. Solids 124 (2019) 634-642.

[24] A. Sarkar, S.A. Maloy, K.L. Murty, Investigation of Portevin-LeChatelier effect in HT-9 steel, Materials Science and Engineering A 631 (2015) 120-125.

[25] S. Allain, O. Bouaziz, T. Lebedkina, M. Lebyodkin, Relationship between relaxation mechanisms and strain aging in an austenitic FeMnC steel, Scr. Mater. 64(8) (2011) 741-744.

[26] J. Brechtl, B. Chen, X. Xie, Y. Ren, J.D. Venable, P.K. Liaw, S.J. Zinkle, Entropy modeling on serrated flows in carburized steels, Materials Science and Engineering: A 753 (2019) 135-145.

[27] A. Sarkar, P. Barat, P. Mukherjee, Multiscale entropy analysis of the Portevin-Le Chatelier effect in an Al-2.5%Mg alloy, Fractals 18(3) (2009) 319-325.

[28] A. Chatterjee, A. Sarkar, P. Barat, P. Mukherjee, N. Gayathri, Character of the deformation bands in the (A + B) regime of the Portevin-Le Chatelier effect in

Al-2.5%Mg alloy, Materials Science and Engineering A 508 (2009) 156-160.

[29] N. Chibane, H. Ait-Amokhtar, C. Fressengeas, On the strain rate dependence of the critical strain for plastic instabilities in Al-Mg alloys, Scr. Mater. 130 (2017) 252-255.

[30] T.A. Lebedkina, M.A. Lebyodkin, T.T. Lamark, M. Janeček, Y. Estrin, Effect of equal channel angular pressing on the Portevin–Le Chatelier effect in an Al_3Mg alloy, Materials Science & Engineering A 615 (2014) 7-13.

[31] M.S. Bharathi, M. Lebyodkin, G. Ananthakrishna, C. Fressengeas, L.P. Kubin, Multifractal burst in the spatiotemporal dynamics of jerky flow, Phys. Rev. Lett. 87(16) (2001) 4.

[32] D. Yuzbekova, A. Mogucheva, D. Zhemchuzhnikova, T. Lebedkina, M. Lebyodkin, R. Kaibyshev, Effect of microstructure on continuous propagation of the Portevin-Le Chatelier deformation bands, Int. J. Plast. 96 (2017) 210-226.

[33] M.A. Lebyodkin, N.P. Kobelev, Y. Bougherira, D. Entemeyer, C. Fressengeas, T.A. Lebedkina, I.V. Shashkov, On the similarity of plastic flow processes during smooth and jerky flow in dilute alloys, Acta Mater. 60 (2012) 844-850.

[34] S. Chen, X. Xie, B.L. Chen, J.W. Qiao, Y. Zhang, Y. Ren, K.A. Dahmen, P.K. Liaw, Effects of temperature on serrated flows of $Al_{0.5}$CoCrCuFeNi high-entropy alloy, Jom 67(10) (2015) 2314-2320.

[35] S.Y. Chen, X. Yang, K.A. Dahmen, P.K. Liaw, Y. Zhang, Microstructures and crackling noise of Al_xNbTiMoV high entropy alloys, Entropy 16 (2014) 870-884.

[36] S. Chen, X. Xie, W. Li, R. Feng, B. Chen, J. Qiao, Y. Ren, Y. Zhang, K.A. Dahmen, P.K. Liaw, Temperature effects on the serrated behavior of an $Al_{0.5}$CoCrCuFeNi high-entropy alloy, Mater. Chem. Phys. 210 (2018) 20-28.

[37] S. Chen, L. Yu, J. Ren, X. Xie, X. Li, Y. Xu, G. Zhao, P. Li, F. Yang, Y. Ren, P.K. Liaw, Self-similar random process and chaotic behavior in serrated flow of high entropy alloys, Sci Rep 6 (2016) 29798.

[38] S.Y. Chen, W.D. Li, X. Xie, J. Brechtl, B.L. Chen, P.Z. Li, G.F. Zhao, F.Q. Yang, J.W. Qiao, P.K. Liaw, Nanoscale serration and creep characteristics of $Al_{0.5}$CoCrCuFeNi high-entropy alloys, J. Alloy. Compd. 752 (2018) 464-475.

[39] J. Brechtl, S.Y. Chen, X. Xie, Y. Ren, J.W. Qiao, P.K. Liaw, S.J. Zinkle, Towards a greater understanding of serrated flows in an Al-containing high-entropy-based alloy, Int. J. Plast. 115 (2019) 71-92.

[40] A. Sarkar, A. Chatterjee, P. Barat, P. Mukherjee, Comparative study of the Portevin-Le Chatelier effect in interstitial and substitutional alloy, Materials Science and Engineering A 459 (2007) 361-365.

[41] S.-D. Wu, C.-W. Wu, S.-G. Lin, K.-Y. Lee, C.-K. Peng, Analysis of complex time series using refined composite multiscale entropy Physics Letters A 378 (2014) 1369-1374.

[42] J. Brechtl, X. Xie, P.K. Liaw, S.J. Zinkle, Complexity modeling and analysis of chaos and other fluctuating phenomena, Chaos, Solitons & Fractals 116 (2018) 166-175.

[43] A. Iliopoulous, N.S. Nikolaidis, E.C. Aifantis, Analysis of serrations and shear bands fractality in UFGs, J Mech Behav Mater 24(1-2) (2015) 1-9.

[44] M. Costa, A.L. Goldberger, C.K. Peng, Multiscale entropy analysis of biological signals, Phys. Rev. E 71(2) (2005) 021906.

[45] M. Costa, A.L. Goldberger, C.K. Peng, Multiscale entropy analysis of complex physiologic time series, Phys. Rev. Lett. 89(6) (2002) 068102.

[46] M. Costa, C.-K. Peng, A.L. Goldberger, J.M. Hausdorff, Multiscale entropy analysis of human gait dynamics, Physica A 330 (2003) 53-60.

[47] X. Xie, PhD Thesis, The Experimental and Theoretical Study of Plasticity Improvement of Zr Based Bulk Metallic Glasses, Materials Science and Engineering, Tennessee-Knoxville, 2015.

[48] W. Li, H. Bei, Y. Tong, W. Dmowski, Y.F. Gao, Structural heterogeneity induced plasticity in bulk metallic glasses: From well-relaxed fragile glass to metal-like behavior, Applied Physics Letters 103(17) (2013) 171910.

[49] W. Li., Y. Gao, H. Bei, On the correlation between microscopic structural heterogeneity and embrittlement behavior in metallic glasses, Sci Rep 5 (2015).

[50] J. Brechtl, H. Wang, N.A.P.K. Kumar, T. Yang, Y.R. Lin, H. Bei, J. Neuefeind, W. Dmowski, S.J. Zinkle, Investigation of the thermal and neutron irradiation response of BAM-11 bulk metallic glass, J. Nucl. Mater. 526 (2019) 151771.

[51] T. Egami, Mechanical failure and glass transition in metallic glasses, J. Alloy. Compd. 509 (2011) S82-S86.

[52] T. Egami, K. Maeda, D. Srolovitz, V. Vitek, Local structure of amorphous metals, Journal De Physique Colloques 41(C8) (1980) C8-272-C8-275.

[53] B. Yuan, J.-J. Li, J.-W. Qiao, Statistical analysis on strain-rate effects during serrations in a Zr-based bulk metallic glass, Journal of Iron and Steel Research, International 24 (2017) 455-461.

[54] W. Zheng, Y.J. Huang, G.Y. Wang, P.K. Liaw, J. Shen, Influence of strain rate on compressive deformation behavior of a Zr-Cu-Ni-Al bulk metallic glass at room Temperature, Metall. Mater. Trans. A-Phys. Metall. Mater. Sci. 42A(6) (2011) 1491-1498.

[55] J. Antonaglia, W.J. Wright, X. Gu, R.R. Byer, T.C. Hufnagel, M. LeBlanc, J.T. Uhl, K.A. Dahmen, Bulk metallic glasses deform via slip avalanches, Phys. Rev. Lett. 112(155501) (2014) 1-5.

Declaration of interests

☒ The authors declare that they have no known competing financial interests or personal relationships that could have appeared to influence the work reported in this paper.

☐The authors declare the following financial interests/personal relationships which may be considered as potential competing interests: